

DOI: 10.13208/j.electrochem.180726

Artical ID:1006-3471(2019)06-0781-11

Cite this: *J. Electrochem.* **2019**, 25(6): 781-791

Http://electrochem.xmu.edu.cn

ZIF-67-Derived Ag/Co-Embedded N-Enriched Mesoporous Carbon for Oxygen Reduction Reaction

DI Zheng-ling^{1,2}, ZHU Jing^{1,2}, DAI Lei^{1,2*}, MENG Wei^{1,2}, LI Yue-hua^{1,2},
HE Zhang-xing^{1,2}, WANG Ling^{1,2}

(1. College of Chemical Engineering, North China University of Science and Technology,
Tangshan 063210, PR China; 2. Hebei Province Key Laboratory of Photocatalytic and
Electrocatalytic Materials for Environment, Tangshan 063009, PR China)

Abstract: Nitrogen-doped porous carbon materials are considered as one of the most promising catalysts for oxygen reduction reaction (ORR). Herein, in order to further improve the activity of the nitrogen-doped porous carbon, Ag/Co bimetal is embedded into nitrogendoped porous carbon to form Ag/Co-embedded nitrogen-doped porous carbon material (AgCo@NC). The AgCo@NC was derived by the wet impregnation of Ag⁺ into ZIF-67 precursor, followed by chemical reduction and a subsequent pyrolysis process under Ar atmosphere at different temperatures (500 °C, 600 °C, 700 °C). The morphologic characterization shows that the Ag/Co nanoparticles were successfully embedded in the mesoporous carbon framework with abundant nitrogen atoms. The electrochemical test results indicate that the AgCo@NC-600 catalyst exhibited the higher onset potential and half-wave potential than thods of others and Pt/C in alkaline media. Furthermore, the AgCo@NC and Co@NC also displayed the higher methanol-tolerance performance than commercial Pt/C.

Key words: oxygen reduction reaction; ZIF-67; N-doped porous carbon; Ag nanoparticles

CLC Number: Q81;O646.54

Document Code: A

Development of the catalytic electrode with excellent activity and stability is one of the committed steps in the electrochemical technologies, such as the energy storage and conversion systems^[1-2]. The oxygen reduction reaction (ORR) as the widely used cathode reaction plays an important role in pursuing high efficiency, low operating temperatures and increased durability for metal-air batteries, fuel cells, chlor-alkali electrolysis and so on^[3-6]. Because of the high overpotential and the sluggish kinetics, the ORR usually has to be catalyzed by precious metal catalysts. Up to now, the commercialized catalysts for ORR mainly are platinum or platinum-based alloy materials^[6-7]. Low reserves in crust and high cost of platinum necessitate searching for new catalyst as alternative^[5-6, 8-9]. The main challenge in the development of non-Pt catalytic materials for ORR is how to enhance

catalytic efficiency and lower cost.

Recently, the metals (Fe, Co, Cu, Mo, Ag etc.) /heteroatoms (N, S, P, B etc.) co-doped porous carbon materials exhibit improved ORR electrochemical activity, which is ascribed to the synergetic effects between the metals and heteroatoms^[10-14]. Among these materials, carbon-based electrocatalysts prepared from metal-organic frameworks (MOFs) have attracted special attention^[15-17]. Firstly, the porous carbon materials can be converted from MOFs through direct carbonization without any template or particular process due to ordered compositions, uniform pore sizes and structural topologies of the MOFs^[18-19]. Secondly, nitrogen can be synchronously doped into the carbon materials due to the rich nitrogen source of the MOFs, which exhibits excellent ORR catalytic properties^[19-22]. Finally, metals can be embedded into the

carbon matrix due to pre-existing central metallic ion and the porous structure^[22]. This metal-embedded and nitrogen-doped carbon materials will provide a large number of active sites and the highly dispersed metal particles in the carbon matrix, which is propitious to the improvement of ORR activity and decrease of the metal dosage^[22-23]. Because of the similar size to carbon atom and the effective improvement in electron transport properties of the carbon material, nitrogen atom is a preferred dopant for enhancing electrocatalytic efficiency in batteries. Moreover, the positive charge density in carbon atom caused by the high electronegativity of nitrogen atom can create active sites for ORR^[20, 23].

Based on the high catalytic activity of silver in alkaline electrolyte for fuel cell, seawater electrolysis and organic halide reduction^[24-28], Moreover, in the use of electrocatalysis, silver nanoparticles require a high degree of dispersion, and their size and shape are important control parameters^[25, 29]. In addition, cobalt (Co) is also proved to have good catalytic performance for ORR^[30-31]. Therefore, silver (Ag) can be introduced into the MOF cavity as a second phase, increasing its dispersion and specific area, while also reducing its size and dosage. In this work, silver particles are introduced into the zeolitic imidazolate frameworks (ZIF-67) cavity using the wet impregnation followed by chemical reduction. And by the subsequent pyrolyzation process, the Ag/Co-embedded nitrogen-doped porous carbon material (AgCo@NC) was obtained. The electrochemical properties of the AgCo@NC composite as the catalyst for ORR were investigated in detail.

1 Experimental

Synthesis of ZIF-67: All chemicals and solvents were purchased from commercial approaches. ZIF-67 was synthesized by co-precipitation at room temperature. 1.455 g of $\text{Co}(\text{NO}_3)_2 \cdot 6\text{H}_2\text{O}$ was firstly dissolved in 40 mL of methanol and 40 mL of absolute ethanol. Secondly, 1.642 g of 2-methylimidazole was also dissolved in 40 mL of methanol and 40 mL of absolute ethanol. Then the two solutions were mixed and magnetically stirred for several minutes. The resultant so-

lution was kept for 48 h. The obtained product was separated by centrifugal and purified by washing thoroughly with alcohol several times to remove residual ions. The ZIF-67 was finally obtained by drying above-mentioned product at 80 °C.

Synthesis of AgCo@NC: The synthesis of Ag@ZIF-67 was firstly performed by wet impregnation followed by chemical reduction method. Briefly, 0.5000 g ZIF-67 was added to 15 mL of absolute ethanol to form suspension of ZIF-67 and 0.0504 g AgNO_3 was dissolved into 15 mL absolute ethanol. Then the AgNO_3 solution was slowly added to the suspension of ZIF-67 and magnetically stirred for 5 hours at room temperature. Afterwards, the obtained precipitate was collected by centrifugal and washed extensively with alcohol for several times. The precipitate was dispersed in 15 mL absolute ethanol to form AgNO_3 @ZIF-67 suspension. In order to prepare Ag@ZIF-67, a facile chemical reduction was used with sodium borohydride (NaBH_4) as a reducing agent. The NaBH_4 solution prepared by dissolving 0.0490 g NaBH_4 into 10 mL of absolute ethanol was slowly added to the above-mentioned suspension of AgNO_3 @ZIF-67 under magnetic stirring at room temperature for 4 hours. The obtained purple-black precipitates were collected by centrifugal and washed extensively with alcohol for several times, and finally dried at 50 °C to obtain Ag@ZIF-67. In order to obtain AgCo@NC, the Ag@ZIF-67 powders were calcined in argon (Ar) atmosphere at different temperatures for 2 h.

Material characterizations: The phase identifications of the different materials were carried out by X-ray diffraction (XRD, D8 Advance, Bruker AXS) with a $\text{Cu } K_\alpha$ radiation source. The morphology of the samples was investigated by scanning electron microscope (SEM, JEOL JSM-IT100) and transmission electron microscope (TEM, JEM-2100). X-ray photoelectron spectroscopy (XPS, AXIS ULTARDLD) was used to further characterize chemical element composition and valence state of the samples. The specific surface area and pore size distribution (PSD) of the

different samples were determined from the nitrogen adsorption/desorption isotherms by using high performance surface and micropore analyzer (BeiShiDe Instrument, 3H-2000PM1).

Electrochemical measurements: Cyclic voltammetry (CV) and linear sweep voltammetry (LSV) measurements were performed in a three-electrode system by the Autolab electrochemical workstation to investigate the electrochemical activities toward ORR. A glassy carbon (GC) electrode modified with various electrocatalysts was used as the working electrode, a Pt electrode as the counter electrode, and a Ag/AgCl (in saturated KCl solution) as the reference electrode. For the preparation of working electrode, approximate 20 mg of each sample was dispersed in 1 mL of ethanol solution and homogenized with ultrasound for 15 min. 25 μL of the mixed solution and 5 μL of 5wt% Nafion aqueous solution was drop-casted onto the surface of the GC electrode, and followed by drying at room temperature. The oxygen reduction activity of the materials was tested in KOH solution saturated with Ar or O_2 .

2 Results and Discussion

The Ag@ZIF-67 materials were prepared by impregnation followed by the wet chemical reduction method, and then converted into AgCo@NC materials by thermal annealing under Ar atmosphere. The morphologies of Ag@ZIF-67 and AgCo@NC were characterized by scanning electron microscopy. As shown in Fig. 1, the Ag@ZIF-67 presents the typical well-defined polyhedral morphology similar to the pristine ZIF-67 material^[18], indicating that the embedding of Ag particles did not alter the structural morphology of ZIF-67. After pyrolysis at 500 $^{\circ}\text{C}$ under Ar atmosphere, the product particles inherited the polyhedral morphology (as shown in Fig. 1B), but became obviously shrunk with the smaller size, which is attributed to the decomposition of MOF ligand during the pyrolysis process. With the temperature increasing, the product particles further shrank (Fig. 1C) and the closely connected particles kept the morphology of pristine MOF well. However, after the MOF was pyrolyzed at 700 $^{\circ}\text{C}$, the morphology of product particles was changed since the polyhedral structure was

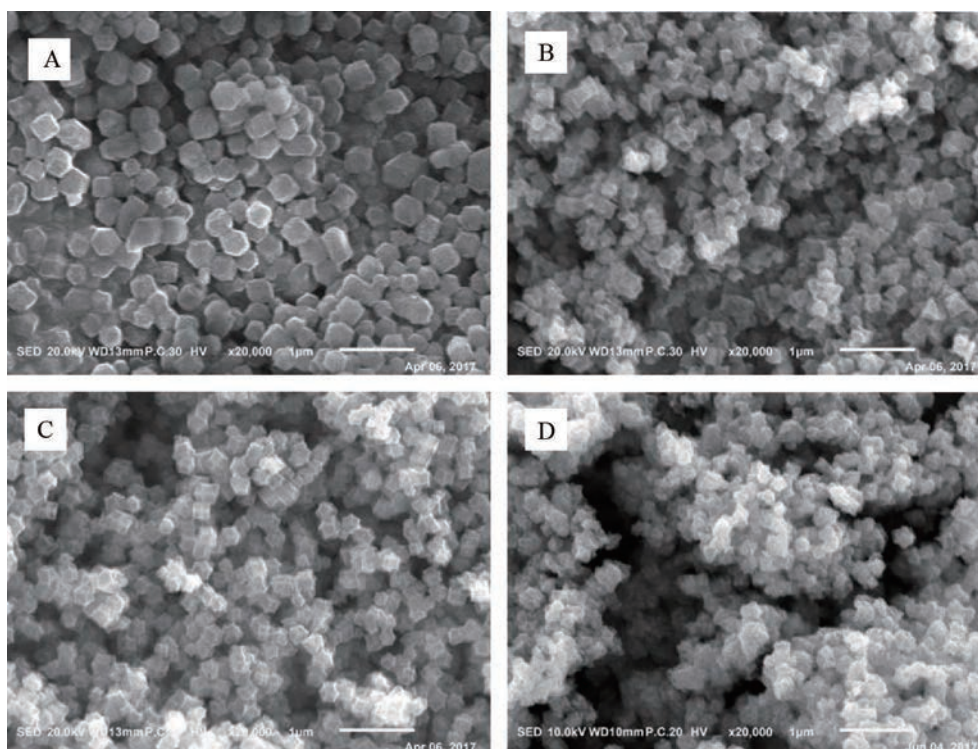


Fig. 1 SEM images of (A) Ag@ZIF-67; (B) AgCo@NC-500; (C) AgCo@NC-600 and (D) AgCo@NC-700

collapsed (Fig. 1D).

Fig. 2A shows the TEM image of Ag@ZIF-67. After ZIF-67 was impregnated by Ag^+ and followed by wet chemical reduction, the Ag nanoparticles (an average size of 10 nm) were encapsulated in the ZIF-67 matrixes. The HRTEM image shows the lat-

tice fringes of the nanoparticles (the inset in Fig. 2A). The 0.236 nm of d-spacing value corresponded to the planes of metallic Ag. TEM image of the Ag-Co@NC-600 sample obtained by *in-situ* thermal decomposition of the Ag@ZIF-67 is shown in Fig. 2B. A lot of nanoparticles are observed in matrix. It can

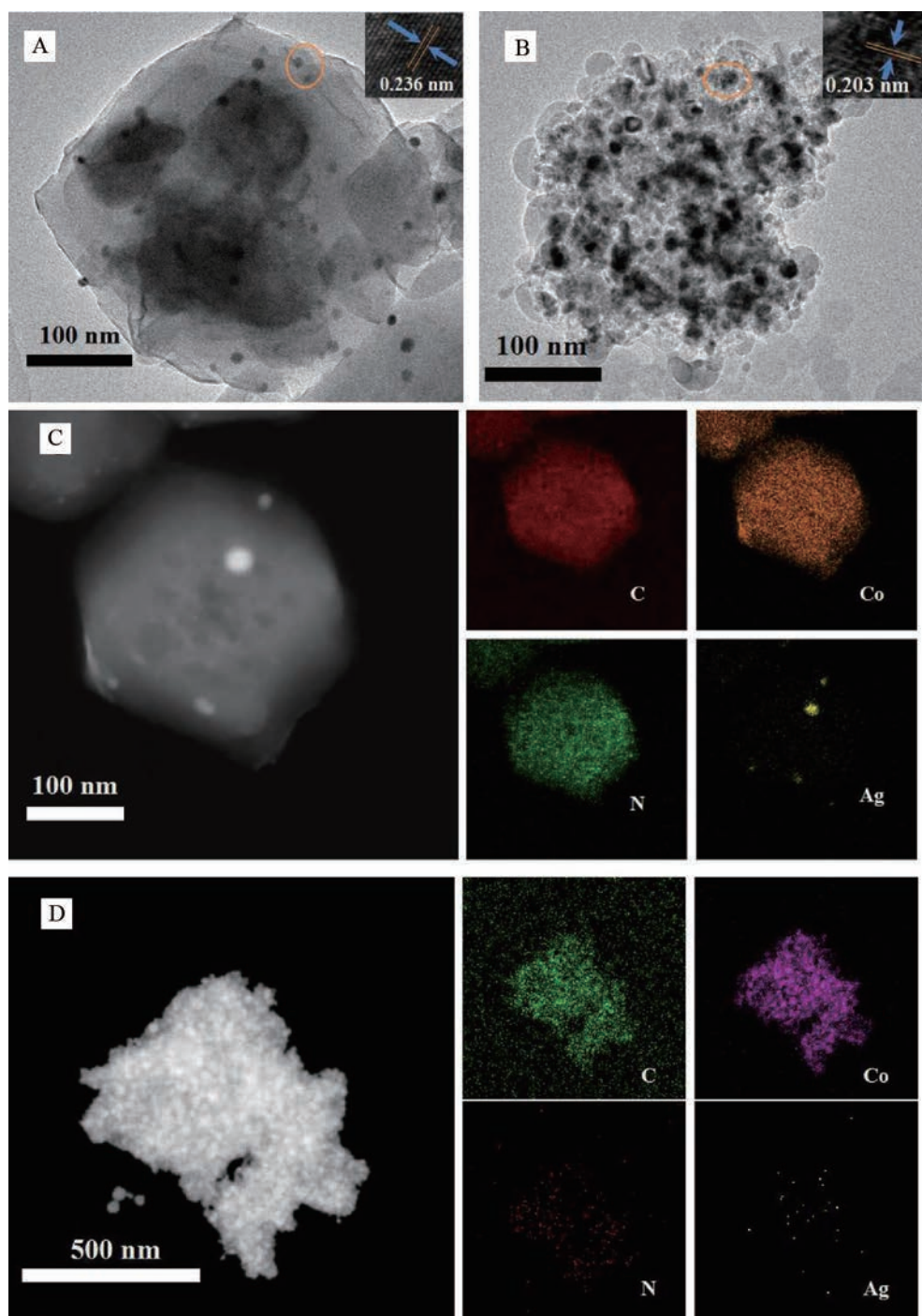


Fig. 2 TEM images of (A) Ag@ZIF-67 and (B) AgCo@NC-600 (the insets: the corresponding particle HRTEM images); STEM-EDX elemental mapping images of C, N, Co and Ag for (C) Ag@ZIF-67 and (D) AgCo@NC-600.

be seen from the HRTEM image (the inset in Fig. 2B) that the particles existing within the carbon matrixes are of 0.203 nm lattice spacing, conforming the presence of Co in terms of the (111) faces. However, only a few Ag nanoparticles are observed in Fig. 2B, which can probably be ascribed to the relatively small amount of Ag particles being easily covered by the Co particles. The elemental mapping images also reveal that Ag was doped into the ZIF-67 (Fig. 2C), while N was uniformly doped into C matrix, and Co and Ag particles were homogenously distributed throughout the C matrix (Fig. 2D). Compared with C and Co, the amounts of N and Ag were low.

Fig. 3 shows the XRD patterns of the products obtained by thermal decomposition of ZIF-67 or Ag@ZIF-67. The XRD pattern of the product from ZIF-67 displays only the peaks assigned to the fcc structured metallic cobalt (the diffraction peaks at 44.3° , 51.6° , and 76.0° , JCPDS Card No. 00-015-0806) and graphitic carbon (the broad peak centered at 26.2° , JCPDS Card No. 00-001-0640), which agreed to the previous report^[32]. For the product from Ag@ZIF-67, except for the peaks of the cobalt and carbon, there also appeared a relatively weak peak located at 38.2° , which is attributed to metallic silver (JCPDS Card No. 01-087-0718). Therefore, it indicates that silver and cobalt particles have been successfully embedded into the carbon matrix to form AgCo@NC.

The porosity of the AgCo@NC-600 material was determined by N_2 adsorption isotherm analysis.

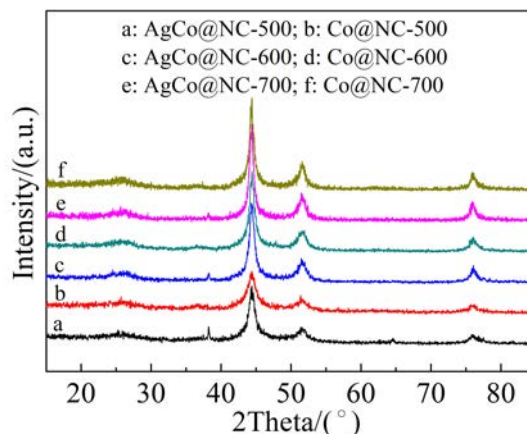


Fig. 3 XRD patterns of Co@NC and AgCo@NC prepared with different carbonized temperatures

The BET surface area of the AgCo@NC-600 material was $245.93 \text{ m}^2 \cdot \text{g}^{-1}$ (Fig. 4A). According to the IUPAC classification, the N_2 adsorption isothermal curve belonged to type-IV isotherm with strong monolayer adsorption at low N_2 partial pressures (< 0.05) and showed the well-defined hysteresis loop at N_2 pressures varying from 0.45 to 1.0, indicating the existence of both micropores and mesopores^[33]. The pore size distribution (PSD) of the AgCo@NC-600 (Fig. 4B) is calculated by density functional theory (DFT) method, which also proves that the AgCo@NC-600 consisted of micropores and mesopores.

The XPS measurement was further performed to obtain the element composition and valence state of the AgCo@NC-600. The survey spectra of AgCo@NC-500, AgCo@NC-600 and AgCo@NC-700

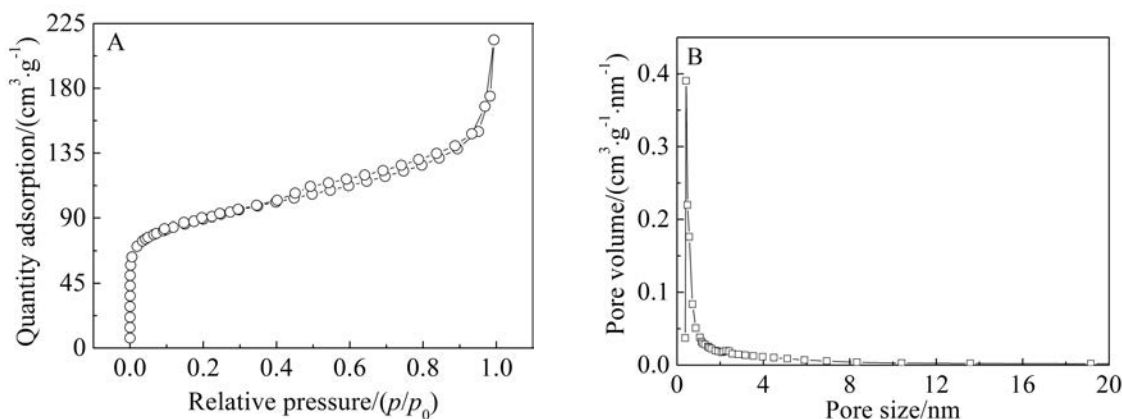


Fig. 4 (A) N_2 adsorption isotherm of AgCo@NC-600; (B) DFT pore size distribution curve of AgCo@NC-600

(Fig. 5A) show the presences of C, Co, N, O and Ag elements, further indicating that the element Ag has been embedded into ZIF-67. The high-resolution Co 2p spectrum of AgCo@NC-600 (Fig. 5B) is separated into five peaks, where the two peaks at about 778.8 eV (Co(0)) and 780.8 eV (Co(II)) are described to Co 2p_{3/2} and the peak at about 796 eV (Co(II)) corre-

sponds to Co 2p_{1/2}^[34-35]. This confirms that part of the cobalt ion is reduced to metallic cobalt during the process of pyrolysis. The two shake-up type peaks at about 786.2 and 803.7 eV are satellite peaks, indicating the presence of Co²⁺ in the sample^[4]. The N 1s spectrum of the AgCo@NC-600 composite is divided into two peaks at 398.9 eV and 401.1 eV (Fig. 5C), attributed

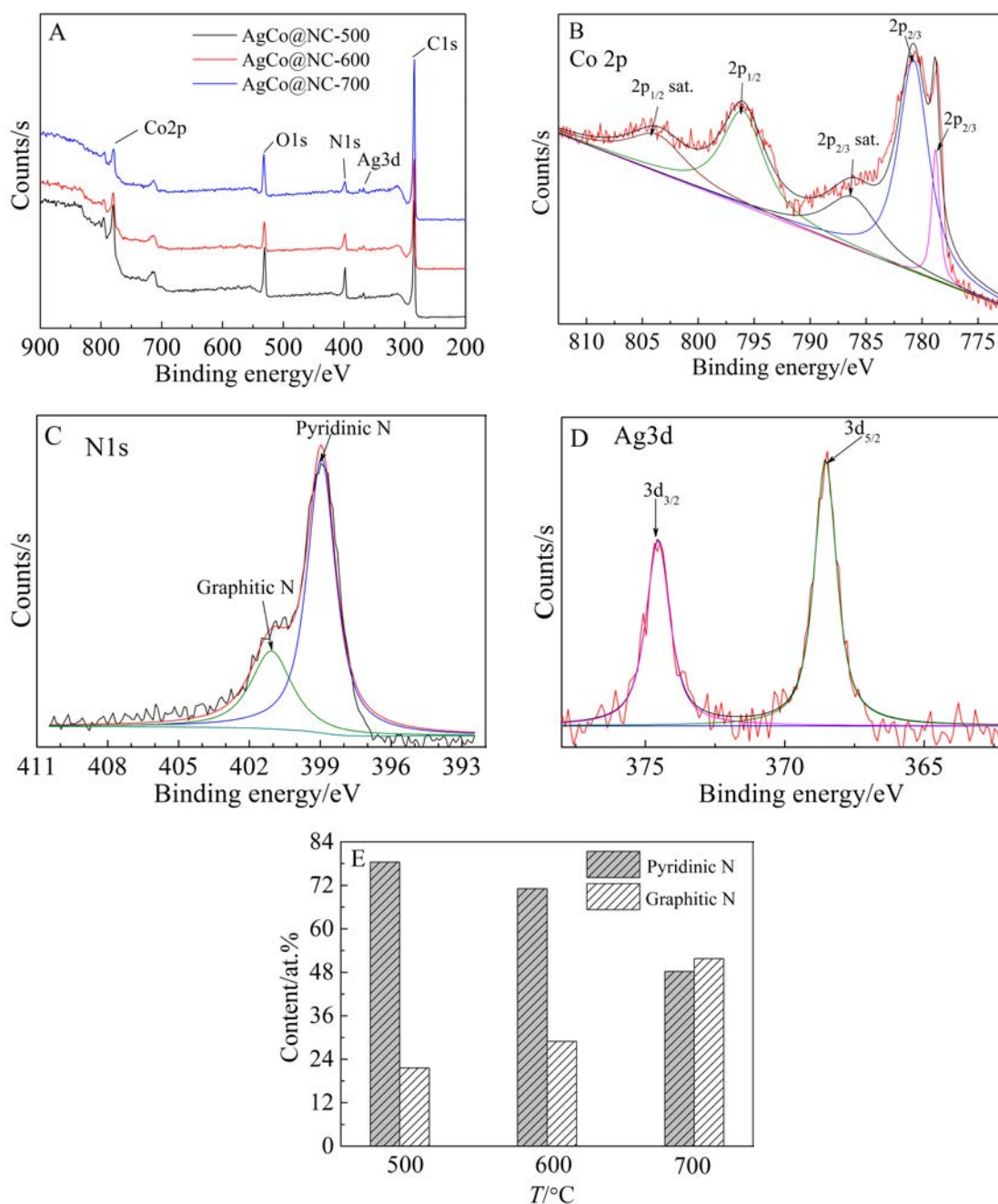


Fig. 5 (A) XPS survey spectra of AgCo@NC-500, AgCo@NC-600, and AgCo@NC-700; the high-resolution XPS spectra of (B) Co 2p, (C) N 1s and (D) Ag 3d for AgCo@NC-600 materials; (E) the relative ratios of pyridinic N and graphitic N at different carbonization temperatures.

to pyridinic and graphitic nitrogen atoms, respectively^[33]. The pyridinic nitrogen formed at low temperatures will be changed into graphitic N with the temperature increasing^[36]. The two types of N species are considered as the efficient ORR-active species^[11-13, 24]. Fig. 5E shows that as the carbonation temperature rose from 500 to 700 °C, the relative percentage of pyridine N decreased, but the graphite nitrogen increased for the AgCo@NC material. The Ag 3d spectrum is divided into two peaks at about 368.5 eV and 374.5 eV (Fig. 5D), which corresponded to Ag 3d_{3/2} and Ag 3d_{5/2}, respectively, assigning to the metal silver. These results further indicate that the Ag and Co particles embed the nitrogen-doped carbon frameworks to form the AgCo@NC material.

Cyclic voltammetry (CV) measurements were conducted to evaluate the ORR activities of the AgCo@NC and Co@NC in Ar or O₂ saturated solutions. As shown in Fig. 6, the CV curve measured in the Ar saturated solution is devoid of any characteristics peak, whereas the CV curve measured in the O₂ saturated 1 mol · L⁻¹ KOH aqueous solution presents a clearly increased cathodic current peak at about 0.26 V attributed to the oxygen reduction process. Fig. 7A shows the comparison of the CV curves for Co@NC and AgCo@NC in the O₂-saturated 1 mol · L⁻¹ KOH aqueous solution. With the introduction of Ag, the cathodic peak of the AgCo@NC is much larger than that of the Co@NC, accompanied by the positive

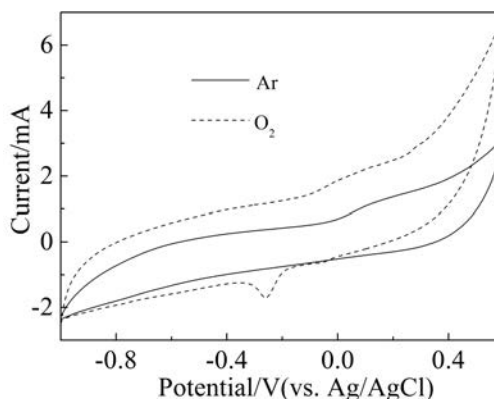


Fig. 6 CV curves of AgCo@NC in Ar and O₂-saturated 1 mol · L⁻¹ KOH aqueous solution with a scan rate of 50 mV · s⁻¹

shift of the peak potential (E_{peak}), indicating the doping of silver can effectively improve the ORR electrocatalytic activity. The electrocatalytic performances of the different samples were compared using rotating ring disk electrode (RRDE) at 1600 r · min⁻¹ in the O₂-saturated 0.1 mol · L⁻¹ KOH aqueous solution. Fig. 7B shows the linear sweeping voltammograms (LSVs) of the Co@NC and AgCo@NC, AgCo@NC-600 ($E_{\text{onset}} \approx 0.012$ V, $E_{1/2} \approx -0.16$ V) exhibits more positive onset potential and half-wave potential than Co@NC-600 ($E_{\text{onset}} \approx -0.087$ V, $E_{1/2} \approx -0.11$ V), also indicating the effective improvement of the activity by the Ag doping.

In order to investigate the influence of pyrolysis temperature on the ORR electrocatalytic activity of

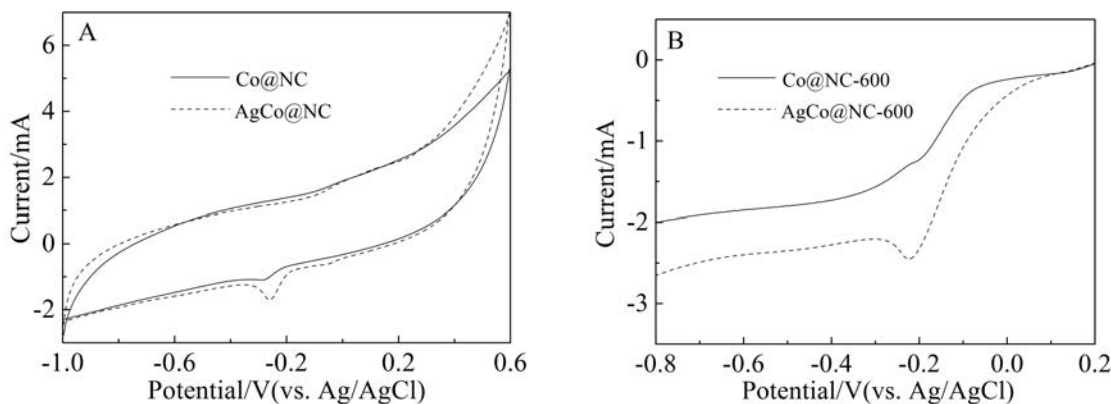


Fig. 7 (A) CV curves of Co@NC and AgCo@NC in O₂-saturated 1 mol · L⁻¹ KOH aqueous solution at a sweep rate of 50 mV · s⁻¹; (B) LSV of AgCo@NC-600 and Co@NC-600 in O₂-saturated 0.1 mol · L⁻¹ KOH aqueous solution at the rotation speed of 1600 r · min⁻¹ with a scan rate of 10 mV · s⁻¹

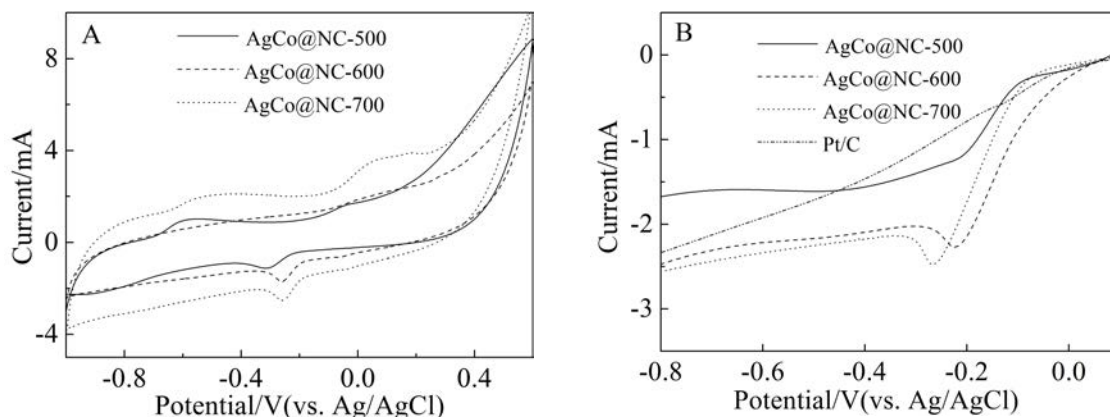


Fig. 8 (A) CV curves of AgCo@NC with different carbonized temperatures in O₂ saturated 1 mol·L⁻¹ KOH aqueous solution with a scan rate of 50 mV·s⁻¹; (B) LSV curves of AgCo@NC with different carbonized temperatures and Pt/C in O₂ saturated 0.1 mol·L⁻¹ KOH aqueous solution at the rotation speed of 1600 r·min⁻¹ with a scan rate of 10 mV·s⁻¹

AgCo@NC, the Ag@ZIF-67 samples were pyrolyzed at 500, 600 or 700 °C. Fig. 8A shows the CV curves of AgCo@NC pyrolyzed at different temperatures in the O₂ saturated 1 mol·L⁻¹ KOH aqueous solution. The CV curves of all the samples present obvious cathodic current peak. It is noted that the E_{peak} of the sample was positively shifted from -0.32 V to -0.26 V when the carbonization temperature was increased from 500 to 600 °C. With further increasing the temperature to 700 °C, the E_{peak} of the AgCo@NC-700 was similar to that of the sample carbonized at 600 °C. In Fig. 8B, AgCo@NC-600 exhibited the most positive onset potential and half-wave potential among these samples and commercial Pt/C catalyst, indicating the best ORR electrocatalytic activity.

In order to assess the ORR stability of the catalyst, 1000 times continual CV measurements for AgCo@NC-600 were conducted between -0.8 and 0.2 V in the O₂ saturated 0.1 mol·L⁻¹ KOH aqueous solution. The LSV curves before and after 1000 cycles of CV measurements are shown in Fig. 9A. It is noted that with the increase of cycle number the half-wave potential of AgCo@NC-600 was shifted negatively about 30 mV after the stability test, which is comparable to those of the materials in previous reports^[15-17, 37]. Furthermore, the methanol tolerance performance of AgCo@NC-600, Co@NC-600 and commercial Pt/C was evaluated by using a chronoamperometry technique. As shown in Fig. 9B, a great change of current was observed over commercial Pt/C after the addition

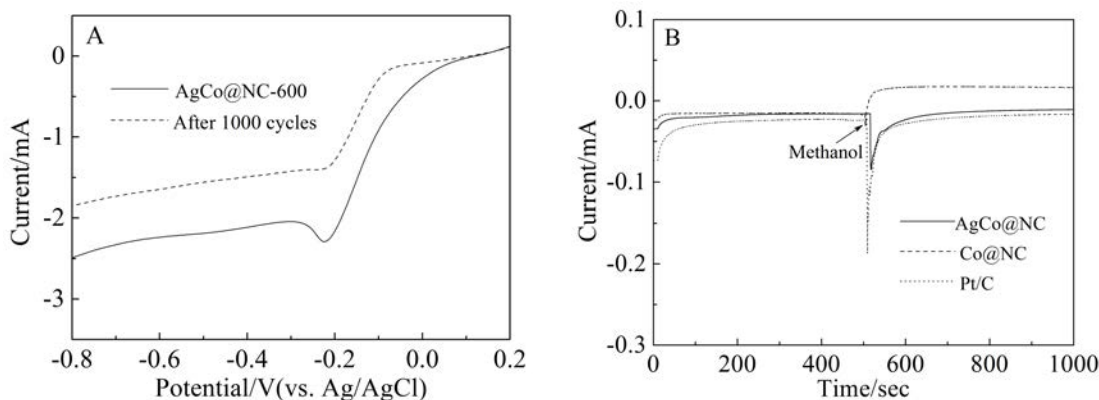


Fig. 9 (A) LSV curves of AgCo@NC-600 in O₂ saturated 0.1 mol·L⁻¹ KOH before and after the 1000 cycles CV test. (B) The chronoamperometric responses of AgCo@NC-600 and Co@NC-600, and commercial Pt/C catalysts at 0.463 V in O₂ saturated 0.1 mol·L⁻¹ KOH solutions followed by a 5-mL methanol injection.

of 5 mL methanol, whereas the currents of AgCo@NC-600 and Co@NC-600 were nearly unchanged under the same conditions, revealing the excellent tolerance of AgCo@NC-600 and Co@NC-600 to methanol crossover effect.

3 Conclusions

A simple and effective approach for preparation of Ag/Co nanoparticles embedded nitrogen doped carbon (AgCo@NC) materials has been successfully developed using ZIF-67 as precursor and nitrogen source. The AgCo@NC exhibited excellent ORR electrocatalytic activity and good durability in alkaline media, which may originate from the bi-metallic catalytic sites, nitrogen dopant and porous structure. Compared with Co@NC and commercial Pt/C, the AgCo@NC catalyst showed higher half-wave potential under the same conditions. This study proposes a new design ideal for efficient enhancement of ORR reaction activity on metal-carbon composites catalyst.

Acknowledgements

The project was supported by the Natural Science Foundation of China (No. 51772097), Hebei Natural Science Funds for Distinguished Young Scholar (No. E2017209079) and Hebei Natural Science Fund (No. B2016209266).

References:

- [1] Zhang Z W, Li H N, Hu J, et al. High oxygen reduction reaction activity of C-N/Ag hybrid composites for Zn-air battery[J]. *Journal of Alloys And Compounds*, 2016, 694: 419-428.
- [2] Men B, Sun Y Z, Tang Y, et al. Highly dispersed Ag-functionalized graphene electrocatalyst for oxygen reduction reaction in energy-saving electrolysis of sodium carbonate [J]. *Industrial & Engineering Chemistry Research*, 2015, 54(30): 7415-7422.
- [3] Wang Y, Lu X J, Liu Y, et al. Silver supported on Co₃O₄, modified carbon as electrocatalyst for oxygen reduction reaction in alkaline media[J]. *Electrochemistry Communications*, 2013, 31: 108-111.
- [4] Wang Y, Liu Y, Lu X J, et al. Silver-molybdate electrocatalysts for oxygen reduction reaction in alkaline media[J]. *Electrochemistry Communications*, 2012, 20: 171-174.
- [5] Wang Y, Liu Q, Zhang L M, et al. One-pot synthesis of Ag-CoFe₂O₄/C as efficient catalyst for oxygen reduction in alkaline media[J]. *International Journal of Hydrogen Energy*, 2016, 41(47): 22547-22553.
- [6] Meng H, Shen P K. Novel Pt-free catalyst for oxygen electroreduction[J]. *Electrochemistry Communications*[J]. 2006, 8(4): 588-594.
- [7] Soo L T, Loh K S, Mohamad A, et al. Synthesis of silver/nitrogen-doped reduced graphene oxide through a one-step thermal solid-state reaction for oxygen reduction in an alkaline medium[J]. *Journal of Power Sources*, 2016, 324: 412-420.
- [8] Ruiz-Camacho B, Martínez Álvarez O, Rodríguez-Santoyo H H, et al. Mono and bi-metallic electrocatalysts of Pt and Ag for oxygen reduction reaction synthesized by sonication[J]. *Electrochemistry Communications*, 2015, 61: 5-9.
- [9] Cheng Y H, Li W Y, Fan X Z, et al. Modified multi-walled carbon nanotube/Ag nanoparticle composite catalyst for the oxygen reduction reaction in alkaline solution[J]. *Electrochimica Acta*, 2013, 111: 635-641.
- [10] Wang Y C, Wu H B, Jiang X E. Facile-green synthesis of nitrogen-doped carbon-supported ultrafine silver catalyst with enhanced electrocatalytic property[J]. *Electrochimica Acta*, 2013, 108(10): 66-73.
- [11] Jiang T T, Wang Y, Wang K, et al. A novel sulfur-nitrogen dual doped ordered mesoporous carbon electrocatalyst for efficient oxygen reduction reaction[J]. *Applied Catalysis B - Environmental*, 2016, 189: 1-11.
- [12] Yu H Y, Fisher A, Cheng D J, et al. Cu, N-codoped hierarchical porous carbons as electrocatalysts for oxygen reduction reaction[J]. *ACS Applied Materials & Interfaces*, 2016, 8(33): 21431-21439.
- [13] Tan C, Wang F, Liu J J, et al. An easy route to prepare carbon black-silver hybrid catalysts for electro-catalytic oxidation of hydrazine[J]. *Materials Letters*, 2009, 63(12): 969-971.
- [14] Xu X H, Tan C, Liu H J, et al. Carbon black supported ultra-high loading silver nanoparticle catalyst and its enhanced electrocatalytic activity towards oxygen reduction reaction in alkaline medium[J]. *Journal of Electroanalytical Chemistry*, 2013, 696(8): 9-14.
- [15] Niu Q J, Guo J X, Chen B L, et al. Bimetal-organic frameworks/polymer core-shell nanofibers derived heteroatom-doped carbon materials as electrocatalysts for oxygen reduction reaction[J]. *Carbon*, 2016, 114: 250-260.
- [16] Lu H S, Zhang H M, Liu R R, et al. Macroscale cobalt-MOFs derived metallic Co nanoparticles embedded in N-doped porous carbon layers as efficient oxygen electrocatalysts[J]. *Applied Surface Science*, 2017, 392: 402-409.
- [17] Long J L, Li R, Gou X L. Well-organized Co-Ni@NC

- material derived from hetero-dinuclear MOFs as efficient electrocatalysts for oxygen reduction[J]. *Catalysis Communications*, 2017, 95: 31-35.
- [18] Jiang M, He H, Yi W J, et al. ZIF-67 derived Ag-Co₃O₄ @N-doped carbon/carbon nanotubes composite and its application in Mg-air fuel cell[J]. *Electrochemistry Communications*, 2017, 77: 5-9.
- [19] Qian Y H, Hu Z G, Ge X M, et al. A metal-free ORR/OER bi-functional electrocatalyst derived from metal-organic frameworks for rechargeable Zn-Air batteries[J]. *Carbon*, 2016, 111: 641-650.
- [20] Ying J, Li J, Jiang G P, et al. Metal-organic frameworks derived platinum-cobalt bimetallic nanoparticles in nitrogen-doped hollow porous carbon capsules as a highly active and durable catalyst for oxygen reduction reaction[J]. *Applied Catalysis B - Environmental*, 2018, 225: 496-503.
- [21] Thomas M, Illathvalappi R, Kurungot S, et al. Graphene oxide sheathed ZIF-8 microcrystals: engineered precursors of nitrogen-doped porous carbon for efficient oxygen reduction reaction (ORR) electrocatalysis[J]. *ACS Applied Materials & Interfaces*, 2016, 8(43): 29373-29382.
- [22] Ahn S H, Manthiram A. Self-templated synthesis of Co- and N-doped carbon microtubes composed of hollow nanospheres and nanotubes for efficient oxygen reduction reaction[J]. *Small*, 2017, 13(11): 160343.
- [23] He L, Weniger F, Neumann H, et al. Synthesis, characterization, and application of metal nanoparticles supported on nitrogen-doped carbon: catalysis beyond electrochemistry[J]. *Angewandte Chemie International Edition*, 2016, 47(48): 12582-12594.
- [24] Zhou X J, Bai Z Y, Wu M J, et al. 3-dimensional porous N-doped graphene foam as a non-precious catalyst for the oxygen reduction reaction[J]. *Journal of Materials Chemistry A*, 2015, 3(7): 3343-3350.
- [25] Lai C L, Kolla P, Zhao Y, et al. Lignin-derived electrospun carbon nanofiber mats with supercritically deposited Ag nanoparticles for oxygen reduction reaction in alkaline fuel cells[J]. *Electrochimica Acta*, 2014, 130: 431-438.
- [26] Cao J Y, Guo M W, Wu J Y, et al. Carbon-supported Ag@Pt core-shell nanoparticles with enhanced electrochemical activity for methanol oxidation and oxygen reduction reaction[J]. *Journal of Power Sources*, 2015, 277: 155-160.
- [27] Cheng Y H, Tian Y Y, Tsang S W, et al. Ag nanoparticles on boron doped multi-walled carbon nanotubes as a synergistic catalysts for oxygen reduction reaction in alkaline media[J]. *Electrochimica Acta*, 2015, 174: 919-924.
- [28] Yasuda S, Furuya A, Uchibori Y, et al. Iron-nitrogen-doped vertically aligned carbon nanotube electrocatalyst for the oxygen reduction reaction[J]. *Advanced Functional Materials*, 2016, 26(5): 738-744.
- [29] Ju J(鞠剑), Chen W(陈卫). Synthesis of silver nanoparticles supported on graphene quantum dots for oxygen reduction reaction[J]. *Journal of Electrochemistry(电化学)*, 2014, 20(4): 353-359.
- [30] Xia W, Mahmood A, Liang Z B, et al. Earth-abundant nanomaterials for oxygen reduction[J]. *Angewandte Chemie International Edition*, 2016, 55(8): 2650-2676.
- [31] Jiang M X(姜梦秀), Zhang J(张晶), Li Y H(李月华), et al. Cobalt-based nitrogen-doped carbon non-noble metal catalysts for oxygen reduction reaction[J]. *Journal of Electrochemistry(电化学)*, 2017, 23(6): 627-637.
- [32] Ai K L, Li Z L, Cui X Q. Scalable preparation of sized-controlled Co-N-C electrocatalyst for efficient oxygen reduction reaction[J]. *Journal of Power Sources*, 2017, 368: 46-56.
- [33] Zhang H Y, Tian Y, Zhao J X, et al. Small dopants make big differences: enhanced electrocatalytic performance of MoS₂ monolayer for oxygen reduction reaction (ORR) by N- and P-doping[J]. *Electrochimica Acta*, 2017, 225: 543-550.
- [34] Wang H H, Wang C N, Liu L, et al. Synthesis of Co-Fe-Pd nanoparticles via ultrasonic irradiation and their electro-catalytic activity for oxygen reduction reaction[J]. *Applied Catalysis A - General*, 2018, 560: 103-110.
- [35] Lu H S, Zhang H, Zhang X, et al. Transformation of carbon-encapsulated metallic Co into ultrafine Co/CoO nanoparticles exposed on N-doped graphitic carbon for high-performance rechargeable zinc-air battery[J]. *Applied Surface Science*, 2018, 448: 369-379.
- [36] Pels J R, Kapteijn F, Moulijn J A, et al. Evolution of nitrogen functionalities in carbonaceous materials during pyrolysis[J]. *Carbon*, 1995, 33(11): 1641-1653.
- [37] Huang X Q, Zhao Z P, Cao L, et al. High-performance transition metal-doped Pt₃Ni octahedra for oxygen reduction reaction[J]. *Science*, 2015, 348(6240): 1230-1234.

ZIF-67 衍生的 Ag/Co@NC 材料及其 氧还原性能的研究

狄正玲^{1,2}, 朱 靖^{1,2}, 戴 磊^{1,2*}, 孟 伟^{1,2},
李跃华^{1,2}, 何章兴^{1,2}, 王 岭^{1,2}

(1. 华北理工大学化学工程学院, 河北 唐山 063210; 2. 河北省环境光电催化材料重点实验室, 河北 唐山 063009)

摘要: 氮掺杂的多孔碳材料可作为氧还原反应的催化剂, 本文借助 ZIF-67 富氮多孔的特殊结构, 采用湿式逐步还原法将 Ag 嵌入 ZIF-67 孔隙内, 然后在 Ar 中碳化成功地制备了 Ag/Co 双金属嵌入的氮掺杂的多孔碳复合材料 (Ag/Co@NC) 作为氧还原反应的催化剂. 为了证明 Ag 的突出作用, 同时在 Ar 中碳化了 ZIF-67 制备了 Co 嵌入的氮掺杂的多孔碳材料 (Co@NC). 利用扫描电子显微镜、透射电子显微镜、X 射线衍射、X 射线光电子能谱以及比表面积分析对材料的显微形貌、物相组成、结构进行分析, 采用循环伏安和线性扫描极化曲线对材料的氧还原催化活性和催化稳定性进行研究. 结果表明, Ag 的嵌入未改变 ZIF-67 的晶体结构, 但是大大提高了材料的氧还原催化活性. Ag/Co@NC 材料的半波电位和起始电位均高于 Co@NC 材料, 且其在 1000 次循环伏安测试前后的半波电位变化仅为 30 mV, 显示出很好的催化稳定性和甲醇耐受性, 可作为燃料电池和金属-空气电池的阴极催化剂.

关键词: 氧还原; ZIF-67; 氮掺杂的多孔碳; 银纳米粒子